Author/s:
Dean, J;Melia, HA;Chantler, CT;Smale, LF

Title:
High accuracy characterisation for the absolute energy of scandium Kα

Date:
2019

Citation:
Dean, J., Melia, H. A., Chantler, C. T. & Smale, L. F. (2019). High accuracy characterisation for the absolute energy of scandium Kα. Journal of Physics B: Atomic, Molecular and Optical Physics, 52 (16), https://doi.org/10.1088/1361-6455/ab29b1.

Persistent Link:
https://hdl.handle.net/11343/348066

High Accuracy Characterisation for the Absolute Energy of Scandium Kα

J W Dean,* C T Chantler*,† L F Smale,‡ and H A Melia§
School of Physics, The University of Melbourne, Melbourne Australia
(Dated: August 13, 2024)

The Kα emission spectrum of scandium (Z=21) has not been measured in absolute energy in over 50 years. At the time the data was reported in 'x units' and the angstrom was not a well defined unit. The reported uncertainty was estimated to be approximately 50 ppm (parts per million) or 0.2 eV. This work reports Sc Kα_1^0 and Kα_2^0 peak energies of 4090.699(10) eV and 4085.926(18) eV, respectively, with estimated standard error uncertainties of 2.4 ppm and 4.4 ppm, and with all component peaks characterised for the first time. The satellite component centroids, line-widths, and relative intensities are determined. An electron gun operating at 20 kV, incident on high purity metals, produces the X-ray fluorescence, which Bragg diffracts via a Germanium (220) crystal to permit high-accuracy measurement of energy. The new profile characterisation combined with the absolute energy calibration provides an important definition for future studies in chemical speciation and condensed matter studies. Furthermore, the methodology described obtains a level of accuracy from relatively low energy X-rays to provide an important insight for future studies in pionic spectra and high-accuracy tests of QED.

I. INTRODUCTION

The energy, line width, and shape of characteristic X-ray radiation has been a major topic in atomic physics research for decades [1]. It offers insight into complex inner-shell interactions of electrons, has application to chemistry [2] and astrophysics [3], and has the potential to test fundamental constraints on quantum electrodynamics (QED) [4–7]. The absolute energy profile for scandium has not been experimentally obtained in over 50 years, since Bearden [1].

Relative measures of energy are more typical in the literature for scandium [8–12]; investigations into phenomena such as the anomalous Z-dependence of the Kα line strengths, anomalous asymmetries, and chemical shifts. These investigations present absolute energy on the x-axis by calibrating the Kα_1 and Kα_2 peaks to the results by Bearden [1].

The $2p_{3/2}$ state has double the degeneracy of the $2p_{1/2}$. This suggests that the ratio of the integrated intensity of the peaks: $I(K\alpha_1) : I(K\alpha_2)$ should be exactly 0.5. Experimentally, and shown in relativistic quantum mechanics (QM), this ratio increases with atomic number [13–15]. This anomalous Z-dependence, and the anomalous asymmetry, are of particular importance across the 3d transition metals ($Z = 21$ to $Z = 30$) because the 3d electrons in particular contribute to the amplitudes and structure in the spectra [16].

Shake processes are the favoured explanation of additional satellite components, non-degenerate to the diagram components, which give rise to the asymmetries [10, 17, 18]. Shake processes occur when an extra electron is excited into a higher shell (shake-up) or into the continuum (shake-off), the transition then takes place in a different potential due to the spectator vacancy.

As the fine structure splitting of the $2p$ shell is a relativistic phenomenon, it scales with Z. Scandium is the lowest Z transition metal, so that the detector resolution and observing separation of K$\alpha_{1,2}$ lines is more challenging than for higher Z metals. Scandium has a further challenge with its relatively low Kα energy, posing some challenge for X-ray diffraction. The analytical methods shown in this work pave the way for high accuracy measurements of energy. These methods can be extended to tests for QED anomalies, such as in the He-like Ti spectra [19].

Theoretical calculations of the Sc Kα energy spectrum are extremely complex due to the open shells, and the lone 3d electron. Recent theoretical calculations involve multi-configurational Dirac Hartree Fock (MCDHF) methods [20]. Comparing theory to the previous absolute energy measurement gives little insight into current relativistic quantum mechanic calculations. With this new measurement, with uncertainties at the 2-4 ppm level, novel MCDHF calculations will offer further insight.

*Electronic address: jonathan.dean@unimelb.edu.au
†corresponding author:chantler@unimelb.edu.au
‡Electronic address: lucasfsmale@gmail.com
§Electronic address: hmelia@student.unimelb.edu.au

II. EXPERIMENTAL SETUP

An electron gun bombards high purity (>99.99 % by mass) samples of elements $Z = 21$ (scandium) and $Z = 22$ to $Z = 25$ (for calibration) in turn to generate the X-ray source. The energy of the electron gun (20 keV) ensures that K-transitions are recorded and stable, towards the sudden impact limit. The electrons are incident on the metal surface at 45^0 to maximise the photons propagated towards the monochromator, at an angle normal to the electron gun. The photons are Bragg diffracted by the Germanium (220) curved crystal monochromator (manufactured and calibrated by the National Institute of Standards and Technology) towards the detector arm, which is set at a Bragg angle of 2θ for the relevant spectrum. Three clinometers give raw output in voltage with reference to the base (B) clinometer, these were placed at the crystal housing (CC) and at the lower (DL) and upper (DU) portions of the detector arm, shown in Fig. 1.

The approach of standards laboratories to measure absolute energy requires a diffracting crystal with calibrated lattice spacing [20–24]. This method is particularly sensitive to thermal expansion, high-level interferometry, crystal strain and source location. While these issues can be accounted for, such as the recent work by Mendenhall et al. [25], it requires a significant run time and financial cost. We apply a method with a curved crystal to obtain a self-consistent result with the calibrated transition energies which is highly robust against geometric and temperature uncertainties.

The curved crystal has radius of curvature such that the Bragg angle for Ti Kα (43.4°) diffraction places the detector on the Rowland circle ensuring focus of the most relevant calibration spectra for this measurement. Diffraction of low energy X-rays from Sc Kα can lead to significant broadening. Having the curved crystal focussed on Ti Kα enables focussed data for scandium, and offers a large set of focussed calibration transitions for good statistics. Beyond the energy of Mn Kβ the spectra recorded would be too defocused by the diffractometer point spread function (PSF) at the detector location (over 30 cm from the Rowland circle). Lower atomic numbers provide X-ray energies too low for a sharp diffraction profiles, and indeed, calcium (Z=20) has a Kα energy uncertainty of roughly 100 ppm which is too large to be used as a calibration.

Also seen in Fig. 1 is an adjustable 'Seeman' wedge, which limits the diffracting region of the crystal, which in turn can alter bandpass, instrumental broadening (vignetting) and other complex systematics. The narrower the wedge, the more parallel the incident photon field, enabling the detector to be further from the Rowland circle with similar resolution. This is essential for transitions further away in energy from Ti Kα. However, too narrow a wedge leads to significant vignetting of the profile, when the spectrum is not a direct convolution of the spectrometer and detector point spread function but instead is truncated to one side. This is a systematic that is dealt with in this work and leads to the final uncertainty reported a factor of 3 lower than if uncharacterised.

We emphasise that the Bearden or other *peak energies*, labelled Kα_1^0, Kα_2^0, Kβ^0, are in no way sufficient to generate an accurate dispersion function. Rather the full component characterisation of each spectrum must be used. For this purpose, we use the component characterisation from Chantler et al. [11], enabling us to use a consistent 6 Voigt characterisation for each profile.

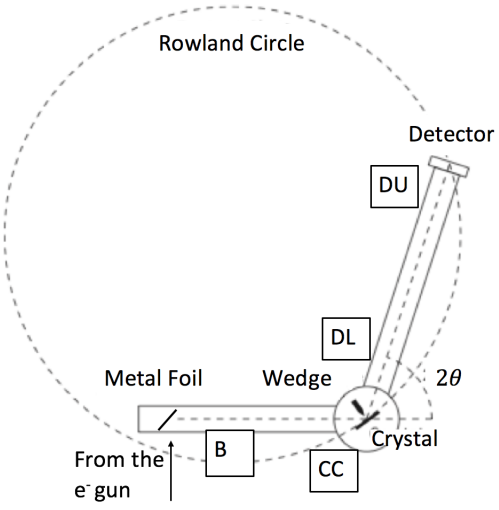

FIG. 1: A schematic diagram of the experimental set-up with the clinometers labels in boxes at their approximate position in the experimental set-up.

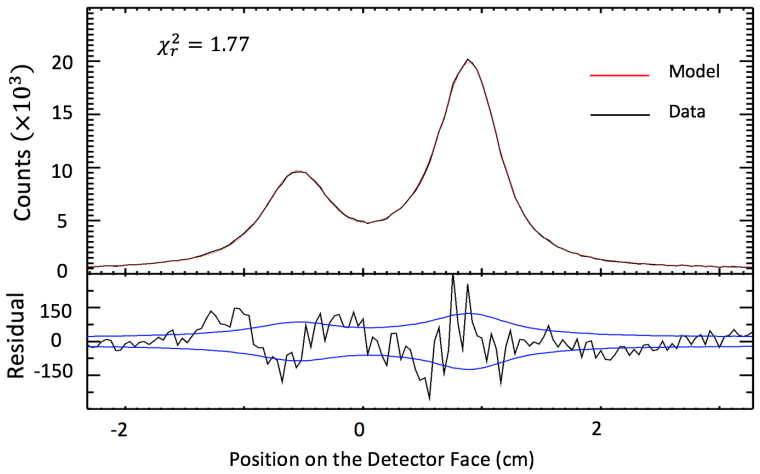

FIG. 2: Raw data profile for a single calibration spectra and the model [11, 15] for Cr Kα, with residual. The χ^2_r value shows the excellent agreement between experiment and model.

The pressure inside the spectrometer (from calibration source to crystal, and crystal to detector) is less than 10^{-7} Torr. Fig. 1 shows a diagram of the set-up with the target element (calibration source), 2θ angle of the arm, Seemann wedge, clinometers and detector.

Our backgammon two-dimensional ion chamber X-ray detector was filled with P10 (10% methane in argon) gas at approximately 1060 Torr (slightly above atmospheric pressure). The value of backgammon detectors has been discussed [26–32].

Key parameters for the X-ray optical geometry are outlined in Table I. Symbols are consistent with [33], Fig. 2:

Name	**Symbol**	**Value**	**Estimated 1σ Uncertainty**
Rowland circle radius	R_z	1121 mm	10 mm
Detector arm length	ZF	1500 mm	5mm
Source to crystal length	BX_z	330 mm	5mm
Source FWHM	sw	5mm	1mm
Crystal thickness	T	0.820 mm	0.005 mm
Electron output shape: Gaussian with FWHM 5 mm			
Three wedge gaps: 2.54(1) mm, 4.58(1) mm, and 14.00(1) mm (fully open)			

TABLE I: Key parameters of the experimental setup with estimated uncertainties.

III. DATA COLLECTION

For each Kα and Kβ transition, 3 runs were performed at each of 3 different wedge positions (2.54mm, 4.98mm, 14.00mm). Run times are roughly 20 minutes each to give the order of 10^4 counts at the peak of the spectra. For each run, the detector arm was shifted slightly so the spectra would be incident on different positions along the detector face: one reading near the centre of the detector face, and one slightly to the left and right. This helps in mapping the dispersion function calibration of the clinometers and in the calibration of the 2θ angle; in identifying vignetted spectra; and to account for electromagnetic edge effects [32].

Fig. 2 illustrates one of the Cr Kα calibration profiles. This is not near the region of Ti Kα and therefore not ideally focussed, yet there is still excellent agreement between the model and the raw data. Some structure in the residual, especially around the maxima of each peak and the minima between the peaks, generally remains within $\sqrt{N}$, the one standard deviation uncertainty envelope. All previous work on the Kα profiles of elements observe similar residual structure with similar χ^2_r including on the much more well-resolved Cu Kα spectrum (e.g. [25] Fig. 18).

IV. DATA ANALYSIS

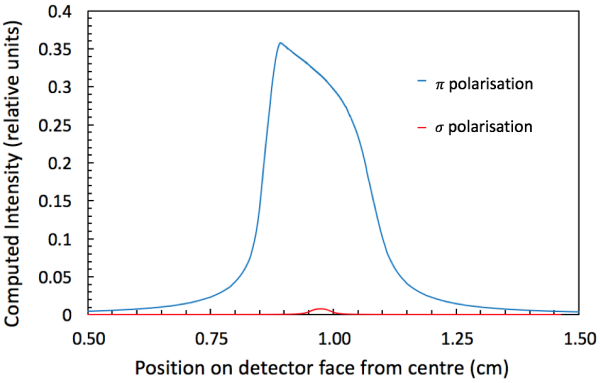

FIG. 3: Theoretical diffraction profile as a function of position on the detector face calculated from *Mosplate* from π and σ polarised photons (at 4090.735 eV) with geometric inputs from table I. The parallel polarised photons (σ) are heavily damped, as expected from a 45° diffracting angle.

The essence of this experiment is to calibrate the spectra to energy. This is done by using the calibration transitions to model a functional that takes clinometry voltage to angle, and curved crystal theory *Mosplate* to map energy to angle. [33–35].

Mosplate diffraction phenomena include refractive index corrections, depth penetration of the wavefield into the crystal, and lateral shifts in position due to X-rays penetrating the crystal. For each energy, a range of spectra are calculated at different crystal angles. A peak position, X, on the detector face is then computed for each of these spectra as a function of E and θ: $X = X_{mos}(E, \theta)$. The model also defines inverse functions that calculate E and θ from the other variables: $E = E_{mos}(X, \theta)$ and $\theta = \theta_{mos}(E, X)$. Significant geometric parameters used by *Mosplate* are given in table I. An example of the calculated diffraction curve is shown in Fig. 3.

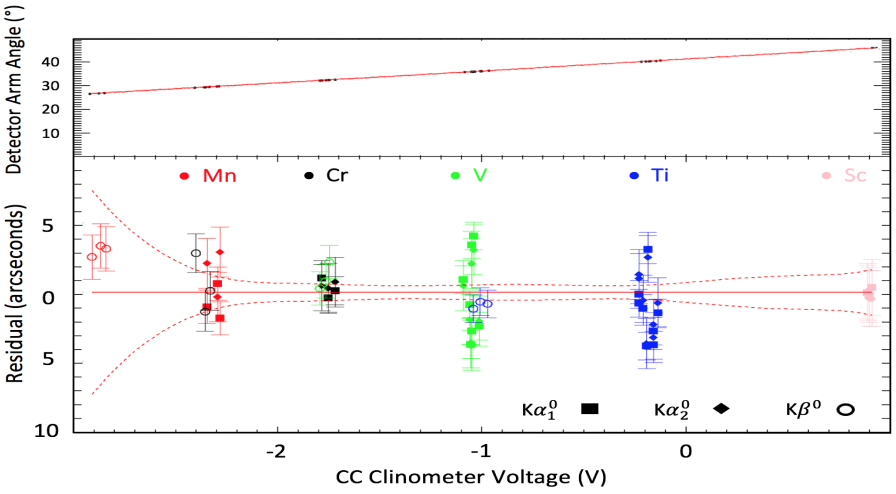

FIG. 4: The dispersion function for one of the clinometers (CC). The residual red-dotted line shows the calculated one standard error uncertainty for the fit extrapolated to the region of Sc Kα energies. The upper plot looks ideal, but the lower expanded plot reveals structure and residuals of the modelling. The residual plot also shows the one standard error uncertainties in the position for each transition centroid. Most of the data points, with their individual fitting uncertainty, lie within the one standard error envelope.

Following the theoretical diffraction modelling, the clinometers are calibrated for angles and energies using K-transitions for elements $Z = 22$ to $Z = 25$ with their 6 Voigt characterisation in [11]. The position on the detector face, the energy of the profile, and the *Mosplate* equation $\theta = \theta_{mos}(X, E)$ are used to give an angle. The angle calibrates the clinometers using a functional $f_{disp}(V) = \theta$ for V, voltage.The absolute energy measurement for scandium can then be found by extrapolating the dispersion function and using the *Mosplate* equation: $E = E_{mos}(X, f_{disp}(V))$. An

example of the dispersion function is shown in Fig. 4. The one standard error uncertainty for the fit of the dispersion function is calculated from the fitted covariance matrix.

A. Vignetting

Vignetting is a common issue with high-resolution spectra and occurs when a slit, or 'Seeman' wedge, is relatively narrow and blocks some of the photons which would be incident upon the diffracting crystal and would otherwise diffract to the detector. This will result in an observed energy separation of the Kα components less than the true value. However, the rectangular slit (wedge) has a very simple transitional form from fully open to fully obstructing, which corresponds to a ramp or triangular function. Hence we apply a linear vignetting function to investigate and model any spectra which might be significantly affected by this.

This function was included in the overall fitting of the spectra as a product, corresponding to a non-uniform convolution function. This gives significant improvements to the χ^2_r measure, up to a factor of three. Furthermore, without the vignetting function correction, the overall fit of the dispersion function (Fig. 4) has a greater value for χ^2_r and the range of the residuals is a factor of two larger for vignetted calibration lines. Without the model correction these lines can be excluded, of course, but the success of the modelling is that this procedure, including or excluding vignetted spectra, is robust down to below 3 parts per million (ppm).

For the larger wedge gaps (4.94 mm and 14.00 mm) vignetting was neither necessary nor observed, and implementing the vignetting functional fit had no effect on profile spectra or χ^2_r. Furthermore, there was no vignetting for the Kβ profiles as expected since they are narrower spectral profiles.

B. Error Budget

Table II presents our final error budget from this experiment. A meticulous error calculation is given in Appendix A.

Error Source	**Estimated 1 standard error uncertainty in this experiment**
Total Sc Kα_1^0	0.010 eV (2.5 ppm)
Total Sc Kα_2^0	0.018 eV (4.4 ppm)
Sc Kα_1^0 statistics	0.005 eV (1.2 ppm)
Sc Kα_2^0 statistics	0.016 eV (3.9 ppm)
Sc Kα Clinometer statistics	0.004 eV (1.0 ppm)
Fitting the dispersion function	0.006 eV (1.5 ppm)
Total Geometry from:	0.0052eV (1.3 ppm)
Rowland circle radius (R_z)	0.0031 eV
Detector arm length (ZF)	0.0038eV
Source to crystal length (BX_z)	0.0015 eV
Wedge width	0.0009 eV
Source FWHM (sw)	0.0005 eV
Crystal thickness (T)	0.0004 eV

TABLE II: The error budget for reported Sc Kα_1^0 and Kα_2^0 values. The individual errors are summed in quadrature to arrive at the final error. The dispersion function uncertainty is dominated by the extrapolation uncertainty.

C. Subset Analysis (Robustness) and Consistency

To ensure that the effect of the vignetting profile or differences between Kα and Kβ characterisations do not affect our results, we obtain the Sc Kα peak energies from 4 different calibration subsets. Table III provides the absolute energies for Sc K$\alpha_{1,2}^0$ for each of the calibration subsets with calculated uncertainty. The range in Kα_1^0 energy is 0.0047eV and for Kα_2^0 is 0.029eV.

Subset of spectra (no.)	Peak i	Centroid C_i, eV
All (54)	$K\alpha_1^0$	4090.699(10)
	$K\alpha_2^0$	4085.926(18)
All Kα (42)	$K\alpha_1^0$	4090.705(15)
	$K\alpha_2^0$	4085.933(28)
All non-vignetted (12 Kβ and 13 Kα)	$K\alpha_1^0$	4090.678(20)
	$K\alpha_2^0$	4085.897(33)
All Kβ (12)	$K\alpha_1^0$	4090.785(45)
	$K\alpha_2^0$	4086.002(101)

TABLE III: For each of the 4 subsets used in calibrating the dispersion function, the final answer for values for the centroid for each component position for Sc Kα are shown. Numbers in parentheses are one standard error uncertainties of the quoted value referring to the last digits.

The 3 clinometers and 3 separate scans of the Sc Kα profile give 9 different results. Remarkable consistency across the values are shown in Figures 5, 6, with all values within one standard error of another.

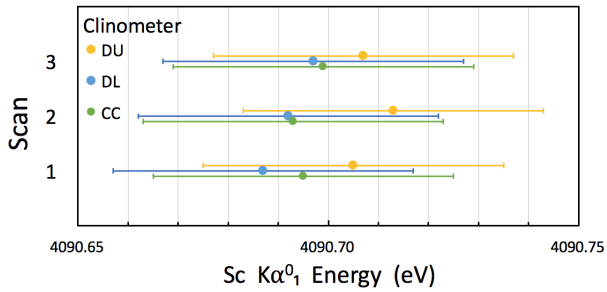

FIG. 5: The values for the centroid of $K\alpha_1^0$ for each of the scans for each clinometer with its respective one standard error uncertainty. Individual uncertainties from statistics on profile, clinometry and dispersion mapping are 6-8 ppm.

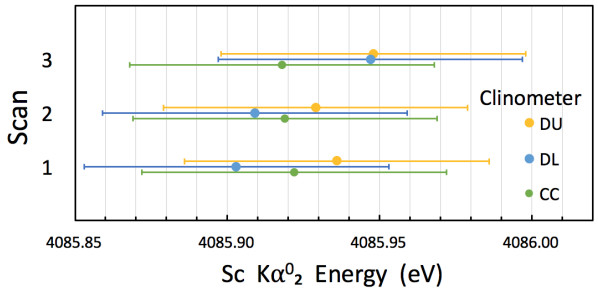

FIG. 6: The values for the centroid of $K\alpha_2^0$ for each of the scans for each clinometer with its respective one standard error uncertainty. Individual uncertainties from statistics on profile, clinometry and dispersion mapping are 10-18 ppm.

V. RESULTS

A. Component fitting

We fit 6 Voigt functions to the Sc Kα profile, with their parameters reported in table IV. A plot with the data and fitted Voigts is shown in Fig. 7.

Fitting of the Voigt profiles is done using the parameters shown in table IV, a common Gaussian width, and a background amplitude. The uncertainties of the parameters are obtained from the diagonal covariance matrix.

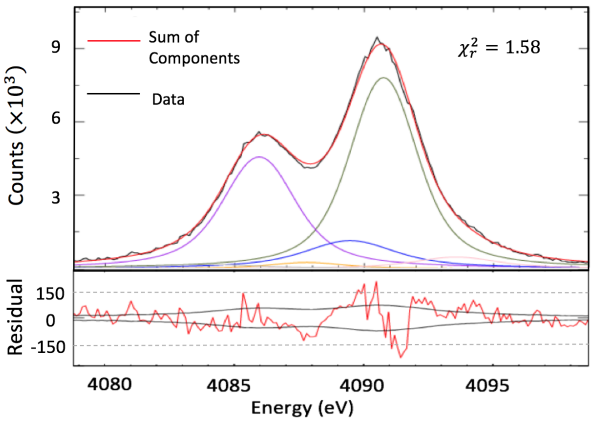

FIG. 7: Fit of the six Voigt profiles for a single spectrum of Sc Kα.

Peak i	Centroid C_i, eV	FWHM W_i, eV	Fraction of integrated area	$E(K\alpha_{jk}) - E(K\alpha_{11})$
Kα_{11}	4090.709(5)	1.15(7)	0.501(21)	0
Kα_{12}	4089.418(103)	2.89(41)	0.107(18)	-1.291
Kα_{13}	4087.752(89)	1.02(82)	0.015(6)	-2.957
Kα_{15}	4093.508(92)	2.01(22)	0.043(8)	+2.799
Kα_{21}	4085.918(16)	1.40(13)	0.321(15)	-4.791
Kα_{22}	4083.926(204)	3.86(92)	0.014(6)	-6.783

TABLE IV: Voigt profile component fit for Sc Kα. Numbers in parentheses are one standard error uncertainties. The common Gaussian width is 0.784(14) eV. Fitting uses initial parameters from [11] and letting independent parameters be free to move. Uncertainties are from fitting three independent scans.

Whilst the last absolute measurement of Sc Kα was some 50 years ago, there have been more recent characterisations in terms of six Voigt profiles to a relative spectrum [9, 11]. We present the differences between these past characterisations and this work in tables V and VI. Comparisons are done after first shifting the previous literature's profile such that the 2 Kα_{11} centroids align. The comparisons are given in terms of absolute values, and as a fraction of the sum of the two 1σ uncertainties.

Peak i	Centroid difference, eV	Width difference, eV	Area difference
Kα_{11}	0	+0.02 (0.17σ)	+0.002 (<0.05σ)
Kα_{12}	-0.002 (<0.05σ)	-0.24 (0.28σ)	-0.002 (0.05σ)
Kα_{13}	-0.006 (<0.05σ)	+0.39 (0.22σ)	-0.001 (0.07σ)
Kα_{15}	+0.003 (<0.05σ)	+0.08 (0.19σ)	+0.005 (0.39σ)
Kα_{21}	-0.013 (0.52σ)	+0.13 (0.65σ)	-0.001 (<0.05σ)
Kα_{22}	+0.014 (<0.05σ)	-0.37 (0.22σ)	-0.005 (0.38σ)

TABLE V: Comparison of this work with Chantler et al. [11, 24]. Differences are expressed in energy and as a sum of the two 1σ uncertainties.

B. Derived peak position, eV

The derived peak positions (eV) for Kα_1^0 and Kα_2^0, averaged over all 9 scans, obtained from the full calibration set are shown in Table VII.

These results are in excellent agreement with the previous experimental results [1]. However, this is not so surprising as Bearden reports a large error bar. A minor discrepancy is seen compared with a previous theoretical calculation [20], difference in results fall just outside of the one standard error region, summarised in table VIII.

One issue plaguing modern atomic physics is the anomalous Z-dependence of the Kα line intensities [13–15]. Our

Label [9] (our label)	ΔE [9] cf. this work, eV (fraction of 1σ)
$K\alpha_{11}$	0
$K\alpha_{12}$ ($K\alpha_{15}$)	+0.016 (0.12σ)
$K\alpha_{13}$ ($K\alpha_{12}$)	+0.088 (0.58σ)
$K\alpha_{21}$	+0.004 (0.17σ)
$K\alpha_{22}$ ($K\alpha_{13}$)	+0.341 (2.1σ)
$K\alpha_{23}$ ($K\alpha_{22}$)	+0.043 (0.19σ)

TABLE VI: Comparison of this work with Anagnostopoulos et al. [9]. Differences are expressed in energy and as a sum of the two 1σ uncertainties. We present their component label and our own in parentheses.

Peak i	Derived Peak energy $K\alpha_i^0$, eV	FWHM W_i, eV	Proportion of integrated area
$K\alpha_1^0$	4090.699(10)	2.636(48)	0.665(9)
$K\alpha_2^0$	4085.926(18)	2.737(60)	0.335(15)

TABLE VII: Derived peak energies, widths, and amplitudes for Sc $K\alpha_1^o$ and $K\alpha_2^0$. Numbers in parentheses are one standard error uncertainties.

Peak i	Measurement , eV	Difference, eV (as a sum of 1σ uncertainty)	Reference
$K\alpha_1^0$	4090.6(2)	-0.099 (0.47σ)	[1]
$K\alpha_2^0$	4086.1(2)	+0.174 (0.80σ)	
$K\alpha_1^0$	4090.15(42)	-0.549 (1.3σ)	[20]
$K\alpha_2^0$	4085.43(44)	-0.496 (1.1σ)	

TABLE VIII: Comparison of derived peak energies for Sc $K\alpha_1^0$ and $K\alpha_2^0$ with experiment [1], and theory [20]. Numbers in parentheses are one standard error uncertainties.

data for the proportion of integrated intensity yield $I(K\alpha_2) : I(K\alpha_1)$ as 0.503(18). Three recent characterisations of the ratio of line intensities yield 0.525(4) [10], 0.52 [9], and 0.51(4) [11]. These are all larger than our value, but within our reported uncertainty. The observed pattern for elements $Z = 20$ to $Z = 80$ strongly suggests a ratio no greater than 0.51, as observed in this work.

VI. CONCLUSION

Novel experimental techniques have been presented, and should be extended to investigations of anomalies in X-ray tests of QED. With similar analytical techniques, it may be possible to reach 1 ppm accuracy. This exciting avenue for future work may reveal new physics. This work shows the reliability of curved crystals in diffraction experiments for spectrometry. The error budget presented shows the robustness of the result to individual geometric uncertainties.

The Sc Kα spectrum has not been subject to an absolute energy calibration for over 50 years. This work reports values 30 times more accurate than previous literature, enabling novel relativistic quantum mechanic calculations to test consistency with experiment. The characterisation of 6 Voigt profiles is highly accurate and gives insight into asymmetries and the ratio of line intensities. The characterisation of component peaks is essential for transferability of standards and for detailed investigation of relativistic quantum mechanics. We report the Sc Kα energy to an accuracy consistent with current state of the art measurements.

References

[1] J. A. Bearden, "X-ray wavelengths," *Rev. Mod. Phys.*, vol. 39, pp. 78–124, Jan 1967.

[2] V. I. Vovna, E. P. Domashevskaya, and A. V. Okotrub, "X-ray and x-ray electron spectroscopy of new materials," *Journal of Structural Chemistry*, vol. 58, no. 6, pp. 1057–1060, 2017.

[3] C. T. Chantler, J. A. Lowe, and I. P. Grant, "Multiconfiguration Dirac-Fock calculations in open-shell atoms: Convergence methods and satellite spectra of the copper Kα photoemission spectrum," *Phys. Rev. A*, vol. 82, p. 052505, Nov 2010.

[4] C. T. Chantler, M. N. Kinnane, J. D. Gillaspy, L. T. Hudson, A. T. Payne, L. F. Smale, A. Henins, J. M. Pomeroy, J. N. Tan, J. A. Kimpton, E. Takacs, and K. Makonyi, "Testing three-body quantum electrodynamics with trapped Ti^{20+} ions: Evidence for a Z-dependent divergence between experiment and calculation," *Physical Review Letters*, vol. 109, no. 15, p. 153001, 2012.

[5] L. F. Smale, C. T. Chantler, and J. A. Kimpton, "Methodology for the characterisation of characteristic spectral profiles, applied to chromium K α," *X-Ray Spectrometry*, vol. 44, no. 2, pp. 54–62, 2015.

[6] J. D. Gillaspy, C. T. Chantler, D. Paterson, L. T. Hudson, F. G. Serpa, and E. Takács, "First measurement of Lyman alpha x-ray lines in hydrogen-like vanadium: results and implications for precision wavelength metrology and tests of QED," *Journal of Physics B: Atomic, Molecular and Optical Physics*, vol. 43, no. 7, p. 074021, 2010.

[7] P. Indelicato and E. Lindroth, "Relativistic effects, correlation, and QED corrections on Kα transitions in medium to very heavy atoms," *Phys. Rev. A*, vol. 46, pp. 2426–2436, Sep 1992.

[8] J. Kawai, E. Nakamura, Y. Nihei, K. Fujisawa, and Y. Gohshi, "Sc Kα , and Kα x-ray fluorescence spectra," *Spectrochimica Acta Part B: Atomic Spectroscopy*, vol. 45, no. 4, pp. 463–479, 1990.

[9] D. Anagnostopoulos, R. Sharon, D. Gotta, and M. Deutsch, "K α and K x-ray emission spectra of metallic scandium," *Physical review. A, Atomic, molecular, and optical physics*, vol. 60, no. 3, pp. 2018–2033, 1999.

[10] Y. Ito, T. Tochio, H. Ohashi, M. Yamashita, S. Fukushima, M. Polasik, K. Słabkowska, L. Syrocki, E. Szymańska, J. Rzadkiewicz, P. Indelicato, J. P. Marques, M. C. Martins, J. P. Santos, and F. Parente, "K$\alpha_{1,2}$ x-ray linewidths, asymmetry indices, and [KM] shake probabilities in elements Ca to Ge and comparison with theory for Ca, Ti, and Ge," *Phys. Rev. A*, vol. 94, p. 042506, Oct 2016.

[11] C. T. Chantler, M. N. Kinnane, C. Su, and J. A. Kimpton, "Characterization of Kα spectral profiles for vanadium, component redetermination for scandium, titanium, chromium, and manganese, and development of satellite structure for Z=21 to Z=25," *Phys. Rev. A*, vol. 73, p. 012508, Jan 2006.

[12] S. P. Limandri, R. D. Bonetto, A. C. Carreras, and J. C. Trincavelli, "Kα satellite transitions in elements with 12 <Z< 30 produced by electron incidence," *Phys. Rev. A*, vol. 82, p. 032505, Sep 2010.

[13] S. I. Salem and P. L. Lee, "Experimental widths of K and L X-ray lines," *Atomic Data and Nuclear Data Tables*, vol. 18, no. 3, pp. 233 – 241, 1976.

[14] J. H. McCrary, L. V. Singman, L. H. Ziegler, L. D. Looney, C. M. Edmonds, and C. E. Harris, "K-fluorescent-X-ray relative-intensity measurements," *Physical Review A*, vol. 4, no. 5, pp. 1745–1750, 1971.

[15] G. Hölzer, M. Fritsch, M. Deutsch, J. Härtwig, and E. Förster, "K$\alpha_{1,2}$ and K$\beta_{1,3}$ x-ray emission lines of the 3*d* transition metals," *Phys. Rev. A*, vol. 56, pp. 4554–4568, Dec 1997.

[16] H. Sorum, "The K X-ray spectra of the 3d transition metals Cr, Fe, Co, Ni and Cu," *Journal of Physics F: Metal Physics*, vol. 17, no. 2, p. 417, 1987.

[17] L. G. Parratt, "Electronic band structure of solids by x-ray spectroscopy," *Reviews of Modern Physics*, vol. 31, no. 3, pp. 616–645, 1959.

[18] C. T. Chantler, J. A. Lowe, and I. P. Grant, "High-accuracy reconstruction of titanium x-ray emission spectra, including relative intensities, asymmetry and satellites, and ab initio determination of shake magnitudes for transition metals," *Journal of Physics B: Atomic, Molecular and Optical Physics*, vol. 46, no. 1, p. 015002, 2013.

[19] A. T. Payne, C. T. Chantler, M. N. Kinnane, J. D. Gillaspy, L. T. Hudson, L. F. Smale, A. Henins, J. A. Kimpton, and E. Takacs, "Helium-like titanium x-ray spectrum as a probe of qed computation," *Journal of physics. B, Atomic, molecular and optical physics*, vol. 47, no. 18, p. 185001, 2014.

[20] R. D. Deslattes, E. G. Kessler, P. Indelicato, L. de Billy, E. Lindroth, and J. Anton, "X-ray transition energies: new approach to a comprehensive evaluation," *Reviews of Modern Physics*, vol. 75, no. 1, pp. 35–99, 2003.

[21] R. D. Deslattes and E. G. Kessler Jr, *Experimental evaluation of inner-vacancy level energies for comparison with theory*, pp. 181 – –235. Atomic inner-shell physics, edited by B. Crasemann, New York: Plenum, 1985.

[22] R. D. Deslattes and A. Henins, "X-Ray to Visible Wavelength Ratios," *Phys Rev Lett*, vol. 31, pp. 972–975, 1973.

[23] E. G. Kessler Jr, S. M. Owens, A. Henins, and R. D. Deslattes, "Silicon lattice comparisons related to the Avogadro project: Uniformity of new material and surface preparation effects ," *IEEE Transactions on Instrumentation and Measurement*, vol. 48, pp. 221–224, 1999.

[24] C. T. Chantler, L. F. Smale, and L. T. Hudson, "X-ray energies," in *International Tables for Crystallography, Vol. C*, ch. 4.2.2, pp. x – y, Dordrecht: Kluwer Academic Publishers, 2018.

[25] M. H. Mendenhall, A. Henins, L. T. Hudson, C. I. Szabo, D. Windover, and J. P. Cline, "High-precision measurement of the x-ray Cu Kα spectrum," *Journal of Physics B: Atomic, Molecular and Optical Physics*, vol. 50, no. 115004, pp. 1–18,

2017.
[26] J. A. Kimpton, M. N. Kinnane, and C. T. Chantler, "Development of backgammon-type multiwire proportional counters for the detection of x rays," *Review of Scientific Instruments*, vol. 77, no. 8, p. 083102, 2006.
[27] R. Allemand and G. Thomas, "Nouveau detecteur de localisation: Le dispositif a jeu de jacquet," *Nuclear Instruments and Methods*, vol. 137, no. 1, pp. 141 – 149, 1976.
[28] G. C. Smith, "High accuracy gaseous x-ray detectors," *Nuclear Instruments and Methods in Physics Research*, vol. 222, no. 1, pp. 230 – 237, 1984.
[29] G. C. Smith, J. Fischer, and V. Radeka, "Resolution for X-rays in gas proportional chambers;," *IEEE Transactions on Nuclear Science*, vol. NS-31, no. 1, pp. 111–115, 1984.
[30] B. Duval, J. Barth, R. Deslattes, A. Henins, and G. Luther, "Position-sensitive x-ray detector," *Nuclear Instruments and Methods in Physics Research*, vol. 222, no. 1, pp. 274 – 278, 1984.
[31] T. Mizogawa, M. Sato, and Y. Awaya, "Application of the MBWC two-dimensional position readout technique to a multi-wire proportional counter," *Nuclear Instruments and Methods in Physics Research Section A: Accelerators, Spectrometers, Detectors and Associated Equipment*, vol. 366, no. 1, pp. 129 – 136, 1995.
[32] H. A. Melia, J. W. Dean, L. F. Smale, A. J. Illig, and C. T. Chantler, "The Latest Backgammon Detector Technology," *X-ray Spectrometry*, p. submitted, 2018.
[33] C. T. Chantler, "X-ray diffraction of bent crystals in Bragg geometry. I. Perfect crystal modelling," *Journal of Applied Crystallography*, vol. 25, no. 6, pp. 674–693, 1991.
[34] C. T. Chantler, "X-ray diffraction of bent crystals in Bragg geometry. II. Non-ideally imperfect crystals, modelling and results," *Journal of Applied Crystallography*, vol. 25, no. 6, pp. 694–713, 1991.
[35] D. Paterson, C. T. Chantler, C. Q. Tran, L. T. Hudson, F. G. Serpa, and R. D. Deslattes, "Absolute calibration of an X-ray spectrometer on the NIST electron-beam ion trap: control, design and systematics," *Physica Scripta*, vol. 1997, no. T73, p. 400, 1997.
[36] C. T. Chantler, L. F. Smale, J. A. Kimpton, D. N. Crosby, M. N. Kinnane, and A. J. Illig, "Characterization of the titanium Kβ spectral profile," *Journal of Physics B: Atomic, Molecular and Optical Physics*, vol. 46, no. 14, p. 145601, 2013.
[37] L. Smale, C. T. Chantler, M. N. Kinnane, J. A. Kimpton, and D. N. Crosby, "Characterization of the kβ spectral profile for vanadium," *Physical Review A*, vol. 87, no. 1, p. 022512, 2013.

Appendix A: Error Analysis

An intrinsic precision and accuracy of a relative measurement and relative component uncertainties is given by the statistics accumulated in the spectrum and the resolution function or full width half maximum (fwhm) of the spectral profile. In this experiment, this is dominated by the integrated intensity in the Kα_1 or Kα_2 peaks (for Sc or the reference calibration lines) or in the Kβ peaks for other reference calibration lines. Typically these spectra have been measured so that $\sqrt{N}$ noise equates to a 0.004-0.008 eV (Sc) or 1 - 2 ppm uncertainty for the spectral peak energies e.g. $E(K\alpha^0_{1,0})$ for each reference calibration line or peak, in each of three independent spectra at different offset angles from the Bragg position, and for each of three sets of clinometry data for each spectrum (Fig. 7). The statistics in the clinometry data are similar in count but narrower in distribution so represent a consistent statistical determination of angle to below this level. Indeed, the clinometry statistics are precise to 0.012 eV or 3 ppm for each spectrum and each clinometer set for scandium (9 data sets for Sc Kα). The standard error for the total data set $\sigma_{se} = \sqrt{\frac{1}{\sum_{i=1}^{n}\sigma_i^2}} \simeq \frac{\sigma_i}{\sqrt{n}}$ is smaller than the standard deviation of each data set σ_i. The clinometry statistics give a standard error of 0.004 eV or 1 ppm.

Equally, the two dominant components, the Kα_{11} and Kα_{21} diagram lines, were determined to 2 - 7 ppm for each spectrum and for each file. Weak components, effectively from satellite contributions, were naturally less well determined and dominated by both statistics and correlations between components as expected. The 3 scans for the Sc Kα profile enable a standard error of order $\sqrt{3}$ smaller than the 1 - 4 ppm level. Hence yielding final standard errors in the fitting of the profile at the 2 - 4 ppm level.

Iff the uncertainty of profile energies from scans is significantly different, i.e. that the χ^2_r would be greater than unity, then Eqn A1 can obtain the mean and standard error in the total Sc Kα fitting statistic:

$$\overline{x} = \frac{\sum_{i=1}^{n}\frac{x_i}{\sigma_i^2}}{\sum_{i=1}^{n}\frac{1}{\sigma_i^2}}; \sigma_{se} = \sqrt{\frac{1}{(n-1)\sum_{i=1}^{n}\sigma_i^{-2}}\sum_{i=1}^{n}(x_i-\overline{x})^2/\sigma_i^2} \tag{A1}$$

For x_i the energy of scan i, σ_i is the standard error in the energy of scan i as required.

The calibration spectra used references from the literature with uncertainties around the 1 - 3 ppm level. However, this is only relevant inasmuch as the dispersion function is stable and reproducible for the different spectra in off-axis

positions, for the function of energy in terms of detector position, and for the function of angle or energy in terms of clinometry angle or voltage.

Important developments in technique and analysis have led to the three clinometers reporting consistent interpretations of the dispersion functions to remarkable accuracy, indeed to below 1 ppm or 0.004 eV in the region of Sc Kα. Critical in this was the approach to event mode of the spectral data to high count-rate, the optimisation of the resolution for the nearby calibration spectra, the collection of high statistics on the clinometry distributions, the novel dense set of calibration lines, and the processing and correction for vignetted profiles.

A key source of error in the experiment is the uncertainty in the fitting of the dispersion function, including all reference data, spectra, clinometry, theoretical spectral profiles and the consistency thereof.

The uncertainty is calculated using $\Delta f^2 = \Sigma Cov(X_i, X_j) \frac{df}{dX_i} \frac{df}{dX_j} \chi_r^2$, from the covariance matrix: $Cov(X_i, X_j) = E[X_i, X_j] - \mu_i \mu_j$ for for X_j one of the variables.

The uncertainty in Fig. 4 is the dashed line above and below the zero error residual line. Unsurprisingly, the uncertainty increases away from the three central calibration lines (Ti, V, Cr). The extrapolation to the Sc region increases the uncertainty further, by approximately a factor of three. This is optimised by having the ideal focus and resolution near Ti Kα, the nearest calibration reference spectra, and equally by having a larger set of Ti calibration spectra, closest to the Sc lines. The uncertainty of the fit for the dispersion function ($f_{disp}(V)$) at the Sc Kα region is the uncertainty that propagates into the dispersion function in the *Mosplate* equation: $E = E_{mos}(X, f_{disp}(V))$. This accounts for the remainder of the uncertainty in the peak energies for the spectrum, namely 0.006 eV for Kα_1^0 and Kα_2^0.

Many systematics are assessed by comparing derived energies and fitting parameters for different spectra and different clinometers. In this experiment, all agree to within 1 standard error, or within 1-2 ppm. This explicitly includes the increased uncertainty due to the extrapolation, and implies that superior results should be obtainable for measurements by interpolation or e.g. for the determination of few-electron transitions and measurements of Quantum Electro-Dynamics (the 1s Lamb shift in medium Z systems, for example).

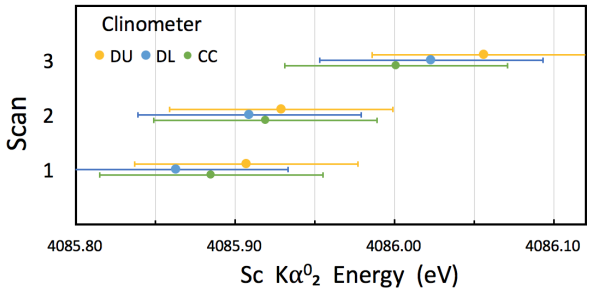

FIG. 8: The values for the centroid of Kα_2^0 for each of the scans for each clinometer with its respective 1σ uncertainty without vignetting corrections.

There is an associated error or uncertainty for the vignetting function used. However, the vignetting function reduces χ_r^2 for all experimental spectra when compared to the current values in literature, and consistently improves agreement in the spectral determination for all data sets, so the error of this appears negligible and rather it reduces all uncertainties and systematics. The vignetting function is essential for experimental setups involving curved crystals, Seemann wedges and data that is 'off-focus'. The vignetting function has been tested for each spectrum (for the narrow 2.14mm wedge) and the results are self-consistent within the set of five elements. When the vignetting function is turned 'off' the dispersion function fits more poorly, and there is a greater spread in values for Kα_1^0 and Kα_2^0 for different scans and data sets (Fig. 8). Discrepancies and excursions occur in the vignetted profiles, so selecting a subset of non-vignetted profiles eliminates any systematic error or uncertainty from this source - and the results and uncertainties are indeed unaffected by adding or subtracting this subset. Indeed, depending on the side of the detector face that the scan is taken, a clear shift of energy is seen on the respective Kα_1^0 or Kα_2^0 line.

Upon correcting for vignetting the agreement of clinometers and spectral energy determinations is perhaps remarkable (Figs 5, 6). These figures summarise the result and consistency from the uncertainties of all spectra, reference and scandium, for the derived peak positions and their stability for each clinometer. The agreement of all lies within 0.002 eV implying the the standard error from these sources will be smaller when pooled.

The greatest sources of uncertainty for this experiment are the scandium profile statistics, the extrapolation of the dispersion function from the region for Ti to Sc (Fig. 4), and the systematic uncertainties due to the uncertainties in the geometric diffraction variables. Consider the effect of a geometric uncertainty (error) on the final measurement of a width, amplitude, component or derive peak energy of scandium Kα. Table I shows the values and uncertainty in each

of the geometric parameters most relevant to the error in *Mosplate*. To arrive at an estimate for a one standard error uncertainty several sets of input parameters are computed and propagated through the analysis, where the parameters are set to their maximal or minimal values as allowed within their uncertainty. Overall, fourteen different sets of input data were used. This alters the three *Mosplate* functions, and importantly the equation: θ: $E = E_{mos}(X, \theta)$. This uncertainty propagates through the dispersion function, when fixing the dispersion function and calculating for final energy, with the nine different sets of input, the centroid of energy for Sc Kα_1^0 and Kα_2^0 would vary at most by 0.009 eV and 0.011 eV respectively. Table II summarises the dominant statistical and systematic uncertainties and errors in our experiment.

Previous application of this detector and spectrometer technology to characterize the profile of Ti Kβ [36] and V Kβ [37] obtained very similar peak statistical uncertainty (1 ppm) and clinometer statistics. The total uncertainty from [37] is 1.3 ppm. However, the final uncertainties from both of those studies were dominated by the robustness of different data sets to 4.5 ppm and 2.7 ppm respectively, or approximately 0.022 eV or 0.015 eV respectively. Conversely in this study, because of the more advanced treatment of the dispersion function and vignetting, all calibration data sets and clinometer dispersion functions are stable and agree within one standard error. In particular, the different sets of wedge data and offset positions in the previous data sets gave significantly different results which we can now interpret to be due to vignetting, the stability of the dispersion function and the modelling of the wedge gaps. In the current investigation, the results for different wedge settings for Ti Kα are all almost consistent, whereas for the earlier work the Kβ wedges gave quite variable answers. Hence an additional systematic error source, although implicit in the robustness of the data sets of the earlier studies, can here be discussed explicitly in terms of the geometric and modelling uncertainties, which of course could be further improved with additional careful investigation.

When comparing the error budget presented here to that of Payne et al. [19], there are a few key differences. The investigation into highly sensitive parameters of QED came with natural experimental difficulties. The statistics on the unknown helium-like spectra at a much lower count-rate, is some 6 ppm in that study whereas it is quite straightforward to obtain a statistical uncertainty for Sc Kα_1 or Kα_2 of 2-3 ppm. The unknown helium-like clinometry statistical uncertainty was 9.7 ppm with a calibration clinometry uncertainty of 7.3 ppm, as compared to the current 1.0 ppm and 1.7 ppm respectively. This is particularly due to an increased event-mode-like clinometry data collection which also collects data at a higher frequency. Uncertainties from shot noise, background and the unknown r-line width are negligible or don't exist in the current experiment, but were significant in the helium-like QED experiment on Ti^{20+}. That detector type used a circular aperture yielding potentially significant 'detector corrections' / uncertainties of 5.1 ppm including in the 'detector fit', compared to an almost negligible uncertainty from all geometric causes in the current experiment [32]. Hence we are able to report an uncertainty of almost an order of magnitude lower than this other experiment.

A great advantage of curved crystal measurement compared with many single or double flat crystal geometries for high accuracy measurement is that any small uncertainty in source or detector location at the micron level leads to shifts in the detection location and often interpreted absolute energy of much larger magnitudes.

An additional major benefit in using the backgammon detector is that it reduces one of the greatest uncertainties of many similar investigations using CCDs or other pixel detectors. The pixel resolution is not a systematic uncertainty for this experiment, as the backgammon detector records a continuum, or analogue, of data points, whereas pixel detectors are limited by their pixel size.

Further advantages of backgammon detectors over pixel based ones include improved energy/flux linearity, and greater damage resistance from X-rays [32]. A further improvement is that our set-up is in a near vacuum state, whereas Mendenhall et al. perform experiments where air absorption is not negligible. Their statistical quality is extremely high (0.05 ppm), though compiled from spectra which do not cover the same energy range, in part to characterise these systematics. Their dependence on temperature and related components have very little effect or uncertainty in our data. Their final quoted uncertainty is 0.13 ppm, dominated by temperature, counting and angle. Our angle uncertainty is given effectively by the dispersion function, so is larger but also dependent upon the statistical data collection of the angular variables.